J Nanopart Res (2015) 17:243
DOI 10.1007/s11051-015-3047-9

RESEARCH PAPER

Carboxymethylated chitosan-stabilized copper nanoparticles: a promise to contribute a potent antifungal and antibacterial agent

Sangeeta Tantubay · Sourav K. Mukhopadhyay · Himani Kalita · Suraj Konar · Satyahari Dey · Amita Pathak · Panchanan Pramanik

Received: 13 January 2015 / Accepted: 20 May 2015

Abstract Carboxymethylated chitosan (CMC)-stabilized copper nanoparticles (Cu-NPs) have been synthesized via chemical reduction of copper(II)–CMC complex in aqueous medium by hydrazine under microwave irradiation in ambient atmosphere. Structural morphology, phase, and chemical compositions of CMC-stabilized Cu-NPs (CMC–Cu-NPs) have been analyzed through high-resolution transmission electron microscopy, field emission scanning electron microscopy, X-ray diffraction, and X-ray photoelectron spectroscopy. Antifungal and antibacterial activities of CMC–Cu-NPs have been evaluated against *Candida tropicalis* and *Escherichia coli* through agar well diffusion method, broth microdilution assay, live–dead assay, and microscopic observation. Antimicrobial activity of spherical CMC–Cu-NPs (~4–15 nm of diameters) has been observed to be significant for both *C. tropicalis* and *E. coli*. The cytotoxicity study indicates that CMC–Cu-NPs have no significant toxic effect against normal cell line, L929.

Keywords Copper nanoparticles (Cu-NPs) · Carboxymethylated chitosan (CMC) · Antifungal · Antibacterial · *C. tropicalis* · *E. coli* · Toxicity study

Introduction

Fungal infections are one of the major causes of global morbidity and mortality, particularly for the patients with weakened immune systems, such as people suffering from acquired immune deficiency syndrome (AIDS) or those subjected to repetitive treatment with antibiotics and chemotherapeutic agents with immunosuppressive activity (Cioffi et al. 2005). The global menace of microbial resistances to common antibiotics (Kyriacou et al. 2004) has led researchers to focus on the development of alternate therapeutic methodology for overcoming these difficulties faced by mankind today. In this regard, use of metal nanoparticles (MNPs) has gained significant relevance since metals and their complexes have been used for their antimicrobial properties for centuries. Small size

Electronic supplementary material The online version of this article (doi:10.1007/s11051-015-3047-9) contains supplementary material, which is available to authorized users.

S. Tantubay · H. Kalita · S. Konar · A. Pathak (✉) · P. Pramanik (✉)
Department of Chemistry, Indian Institute of Technology Kharagpur, Kharagpur 721302, West Bengal, India
e-mail: ami@chem.iitkgp.ernet.in

P. Pramanik
e-mail: ppramanik1946@yahoo.in; pramanik1946@gmail.com

S. Tantubay
e-mail: sang.chem2@gmail.com

S. K. Mukhopadhyay · S. Dey
Department of Biotechnology, Indian Institute of Technology Kharagpur, Kharagpur 721302, West Bengal, India

Published online: 02 June 2015

and large surface areas of the MNPs facilitate their intimate interaction with the microbial cell surfaces and hence are likely to show enhanced antimicrobial activities along with multilevel antimicrobial effects (Jain et al. 2009; Zhao et al. 2010) on cells instead of a single, site-specific interaction observed in case of most of the antibiotics.

Most of the reported antimicrobial studies involving MNPs have so far mainly been confined to the use of silver (Azocar et al. 2014; Chudasama et al. 2010; Kahrilas et al. 2014; Martinez-Castanon et al. 2008; Panacek et al. 2006; Ferrer et al. 2012; Song et al. 2012; Panacek et al. 2009), few on copper (Basumallick et al. 2014; Chatterjee et al. 2012; Cioffi et al. 2004, 2005; Wei et al. 2010), and least on gold (Moreno-Alvarez et al. 2010; Zhao et al. 2010); however, the cost and the availability of Ag pose a major hindrance to its applications. In this pursuit, nanoparticles (NPs) of Cu (the other coinage metal apart from Au and Ag) have been realized as a viable alternative, keeping in mind that people in ancient times used containers made of Cu and Cu-alloys for preserving water and food, the main transmitters of pathogen for most microorganisms borne diseases.

Researchers have synthesized Cu-nanomaterials through different physical and chemical approaches (Chatterjee et al. 2012). Among the different reported approaches, the widely accepted solution-based chemical precipitation method generally involves the precipitation of Cu-NPs or Cu-nanocomposites through reduction of copper salts at optimal precursor concentrations under inert atmosphere (Ar or N_2). Here the particle size of Cu-NPs is manipulated by controlling the process parameters, whereas their stability is often achieved through the use of various stabilizing agents (added in appropriate solvent medium), such as starch (Valodkar et al. 2012), gelatin (Chatterjee et al. 2012), chitosan (Usman et al. 2013), sodium dodecyl sulfate (Soomro et al. 2013), cetyltrimethylammonium bromide (Wu and Chen 2004), and so on (Mott et al. 2007; Song et al. 2004; Zhang et al. 2014; Pulkkinen et al. 2009; Wang and Asefa 2010; Giuffrida et al. 2008; Sarkar et al. 2008; Deng et al. 2013). Their presence in solvent medium during the preparation not only helps in preventing surface oxidation of the Cu-NPs to form Cu_2O and CuO but also helps in controlling their particle size to obtain stable, colloidal dispersions. In view of biological application, it is however more relevant to obtain stable, aqueous dispersions of Cu-NPs using biocompatible, water-soluble polymers as stabilizing agents. Besides, the biocompatible moieties functionalize the surfaces of Cu-NPs and make Cu-NPs more suitable for various biological applications. In this regard, carboxymethylated chitosan (CMC) is an important choice because of its biocompatibility, bio-degradability (Mourya et al. 2010), good water solubility, availability (CMC is derivative of chitosan, and chitosan is synthesized from chitin, the second most abundant naturally occurring polymer), and good chelating ability via the reactive carboxyl, hydroxyl, and amine groups existing in its skeleton. Though CMC has been used as a stabilizing agent to obtain stable dispersions of NPs of various metals and metal oxides, such as Fe_3O_4, Pt, Au, and Ag (Laudenslager et al. 2008; Zhang et al. 2008), use of CMC for stabilizing Cu-NPs is still quite uncommon (Gu et al. 2007) and not much explored. Therefore, in the present study, attempts have been made for the synthesis of CMC-stabilized Cu-NPs through aqueous-based chemical approach where the Cu-NPs get formed in situ through reduction of Cu(II) species by hydrazine (N_2H_4) in the presence of CMC under microwave irradiation in ambient environment. Here, CMC is used as a stabilizing agent that assists in obtaining stable, aqueous colloidal dispersion of Cu-NPs. Facile synthesis of CMC-stabilized Cu-NPs (CMC–Cu-NPs) produces particles of high-quality, while most of the existing methods (Chatterjee et al. 2012; Usman et al. 2013) of Cu-NPs synthesis produce particles having limited stability and/or poor aqueous dispersibility in time-consuming way (For comparison with other methods, see Section 1 under 'Supplementary Material 1').

Antibacterial activity of CMC-stabilized Cu-NPs has been tested against *Escherichia coli*. The present study also reports its antifungal efficiency toward *Candida tropicalis* since, most of the previously reported antimicrobial studies involving Cu-NPs or, Cu-nanocomposites-films/NPs have been restricted only to select bacterial species (Chatterjee et al. 2012; Jia et al. 2012; Mallick et al. 2012), while their antifungal activity (Cioffi et al. 2004, 2005; Wei et al. 2010) and the mechanism of their interaction have remained fewer and inconspicuous till date. *Candida tropicalis* is the most prevalent pathogenic yeast, which shows high resistance to antifungal drugs and is responsible for septicemia and disseminated

candidiasis in tropical countries, especially in patients with lymphoma, leukemia, and diabetes (Powderly et al. 1999; Rippon 1988).

Among the various reports on the synthesis of Cu-NPs, our procedure being probably one of the simplest ones offers much improved stability and aqueous dispersibility. Surface stabilization of Cu-NPs with CMC reduces the potential health risks of CMC-stabilized Cu-NPs. Therefore, ease of synthesis, prevention of surface oxidation, stable dispersions, and very strong antimicrobial activity without significant toxicity (most important) distinguish our work from previous ones. The present study has been focused on the synthesis of CMC–Cu-NPs and chemical characterization of the NPs through XRD, FT-IR, HRTEM, FESEM, TGA etc. along with the screening of its antimicrobial potency against human pathogens and evaluation of its cytotoxicity against normal cells.

Experimental section

Synthesis of carboxymethylated chitosan (CMC)

CMC was prepared with modification of the method reported by Chen and Park (2003). In this modified procedure, at first 2 g of chitosan was suspended in 15 mL of 40 % (w/v) aqueous solution of NaOH and kept at 0 °C for 8 h. The cold alkaline mixture was then transferred to 60 mL of 2-propanol and subsequently 6 g mono-chloroacetic acid (dissolved in 2 mL isopropanol) was slowly added into it within 30 min. The entire mixture was stirred at 28 °C (i.e., room temperature) for 12 h. Eventually, the reaction was stopped by adding 50 mL of 70 % ethanol into the mixture, and the obtained white solid mass of CMC (i.e., the sodium form of CMC) was separated by centrifugation and washed with 80–90 % ethanol. Any trace of unreacted chitosan in the white solid was removed by dissolving it in water and re-precipitating it by addition of anhydrous ethanol. The purified precipitate of the sodium form of CMC was then vacuum-dried at 50 °C for 12 h.

Synthesis of CMC-stabilized Cu-NPs

For the synthesis of CMC-stabilized Cu-NPs (CMC–Cu-NPs), at first 25 mL of 0.32 M aqueous copper(II)sulfate pentahydrate solution and 100 mL of 0.4 % (w/v) aqueous CMC solution were mixed together at 28 °C and the pH of the resultant light-blue dispersion was adjusted to 9. Subsequently, 5 mL hydrazine was added quickly into the reaction mixture and resultant blackish dispersion was subjected to microwave irradiation for 2 min at 600 W powers using a domestic microwave oven. The color of the mixture changed from blackish to the characteristic wine-red color of metallic Cu-NPs, indicating the formation of CMC–Cu-NPs. The wine-red colored dispersion of CMC–Cu-NPs was first lyophilized and the obtained fine powder was repeatedly washed with 50 % ethanol and eventually vacuum-dried at 40 °C for 12 h at a vacuum of 15 mm Hg. The main steps of the synthesis of CMC–Cu-NPs have been presented in Fig. 1.

Antimicrobial activity assays

Antimicrobial screening: agar well diffusion method

The antimicrobial property of CMC-stabilized Cu-NPs was evaluated against human pathogens *C. tropicalis* (NCIM 3110) and *E. coli* (ATCC 25922). Sabouraud dextrose medium (Himedia) and nutrient medium (Himedia) were used for all antifungal and antibacterial assays, respectively. The preliminary antimicrobial susceptibility of CMC-stabilized Cu-NPs was tested by agar well diffusion method as described by Perez et al. (1990). Briefly, the microbial isolates were first grown in a broth medium for 12–18 h and then 100 µL of the standardized cell suspensions of 10^6 CFU/mL were spread on agar plates. Agar medium was punched with 6-mm-diameter wells by cork borer and filled with the aqueous dispersion of CMC-stabilized Cu-NPs (2 mg/mL) and precursor control solutions i.e., aqueous solutions of $CuSO_4{\cdot}5H_2O$ (8 mg/mL) and CMC (1 mg/mL). Experiments were performed in triplicate and plates were incubated at 37 °C for 16 h. Following incubation, the zones of inhibition were observed.

Broth microdilution assay

The antimicrobial activity of CMC-stabilized Cu-NPs against the tested microbes was determined by broth microdilution method according to Clinical and Laboratory Standards Institute (CLSI) guidelines

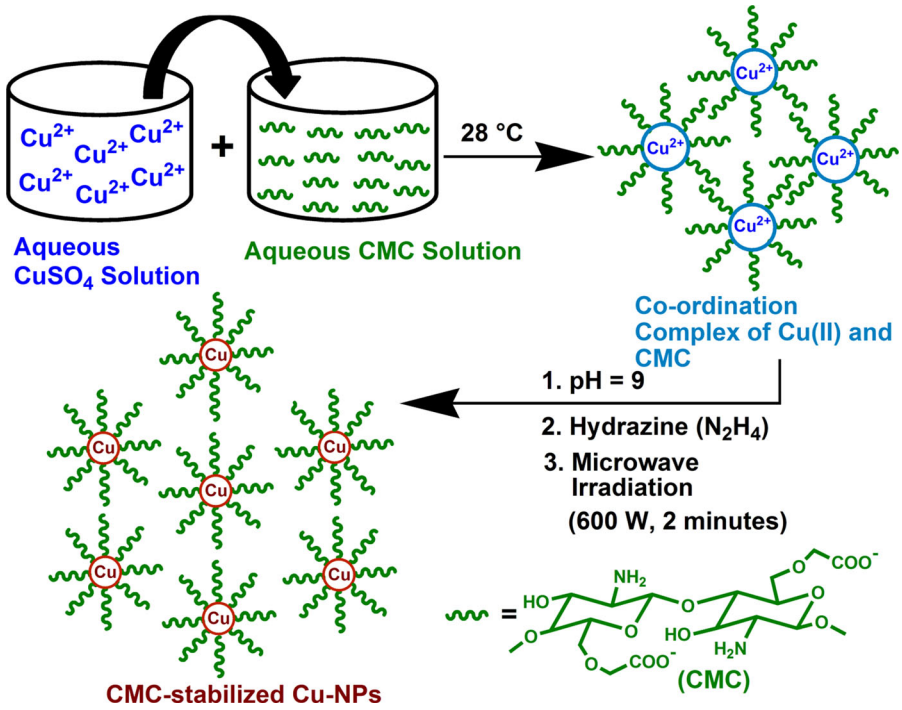

Fig. 1 Schematic representation of the synthesis of CMC-stabilized Cu-NPs

(CLSI 2007). The mid-logarithmic phase microbes were obtained by growing microbes in broth medium, and then diluted in the same medium to obtain approximately 10^6 colony-forming units (CFU)/mL. Aliquots (150 µL) of suspensions containing microbes in culture medium were added to 150 µL of the aqueous dispersions of CMC-stabilized Cu-NPs, and they were successively diluted from 62.5 to 0.12 µg mL^{-1}. The inhibitions of growth were determined by measuring the absorbance of each concentration at 600 nm with a microplate reader after an incubation of 16 h at 37 °C. Microbial growth inhibition was calculated using the following formula:

$$\text{Inhibition } (\%) = 100 - \left(\frac{A2}{A1} \times 100\right),$$

where $A1$ is the absorbance of bacterial cells in control medium and $A2$ is the absorbance of bacterial cells in test medium.

Microscopic observation for antimicrobial activity

The effects of CMC-stabilized Cu-NPs against the tested microbes were studied microscopically by field emission scanning electron microscope (FESEM) (Carl Zeiss SMT AG, Germany: SUPRA 40) and atomic force microscope (AFM) (Agilent Technologies USA: AFM 5500). For FESEM, microbial cultures were placed on glass cover slips and dried under vacuum. Thereafter, dried cells were fixed onto a graphite stub and kept in an auto-sputter coater (E5200, Bio-Rad) under vacuum up to 150 s for gold coating. Images were captured with an accelerating voltage of 5 kV. In AFM analysis, the samples were prepared following the method of Bolshakova et al. (2004). In brief, the droplets of 5–10 µL microbial cell suspensions (10^4 cells/mL) were placed onto the glass cover slips and left to expose for 15 min. Imaging was done using the Pico image basic software.

Live–dead assay

Live–dead assay was performed by live/dead viability assay kit (invitrogen), as per manufacturer's protocol. In brief, both controls and CMC-stabilized Cu-NPs-treated cells were washed with phosphate buffer saline (PBS), and 3 µL of dye mixture (SYTO9 480/500 and PI 490/635) was added to each mL of cell suspension. Mixtures were incubated at 25 °C in dark for 15 min. Thereafter, 5 µL of stained cell suspension was

trapped between a slide and an 18 mm^2 cover slip. Imaging was done using a fluorescence microscope (IX 51, Olympus) and a high-performance CCD camera with the appropriate filter using Image-Pro discovery 5.1 software.

Results and discussion

Characterizations of CMC-stabilized Cu-NPs

Phase analysis

Formation and the stability of CMC-stabilized Cu-NPs were confirmed through XRD phase analysis. A typical X-ray powder diffraction pattern of CMC-stabilized Cu-NPs as depicted in Fig. 2A(a) shows the characteristic diffraction peaks of metallic copper with face-centered cubic (FCC) lattice structure and Fm3 m space group (225). All the observed diffraction peaks can be indexed according to Joint Committee for Powder Diffraction Studies (JCPDS), File No. 04–0836. Sharp XRD peaks indicate the crystalline nature of Cu-NPs. The crystallite sizes of Cu-NPs have been calculated using the Debye–Scherrer equation, given as follows:

$$D = \frac{0.9\lambda}{\beta \cos\theta},$$

where D is the crystallite size, λ is the wave length of the target material ($\lambda = 1.5425$ Å), β is the full width at half height (FWHH) in radians, and θ is the diffraction angle. The average crystallite size is found to be $\sim$21.35 nm. Thus, it can be inferred that the CMC-stabilized Cu-NPs contained pure Cu without any impurity secondary phase (such as CuO, Cu_2O, or $Cu(OH)_2$). To check the stability of Cu^0 in CMC-stabilized Cu-NPs, XRD studies were carried out after the sample was stored for 60 days [depicted in Fig. 2A(b)]. Absence of any impurity phase indicates that the CMC-stabilized Cu-NPs were stable against oxidation up to 60 days, possibly due to the presence of the protective polymer on the surface.

Functional group analysis

Surface modification of Cu-NPs with CMC has been confirmed by comparing the FT-IR spectra of pure CMC and CMC-stabilized Cu-NPs, which are depicted in Fig. 2B(a, b), respectively. The characteristic FT-IR bands (Ge and Luo 2005; Mourya et al. 2010; Prabaharan and Gong 2008) observed in pure CMC at 3446 cm^{-1} (overlapping of O–H and N–H axial stretching vibrations), 1602 cm^{-1} (coupling of angular deformation of N–H bonds of the amino groups and asymmetric stretching vibrations of the carboxylate ions), 1411 cm^{-1} (carboxymethyl groups; symmetric stretching vibrations of carboxylate ions.), and 1070 cm^{-1} (C–O stretching vibrations) are found to be broadened and shifted to lower wave numbers (i.e., $\bar{u} = 3421$, 1597, 1377, and 1053 cm^{-1}, respectively) in CMC-stabilized Cu-NPs, signifying interaction of CMC with the surface of Cu-NPs through its (CMC) carboxyl, hydroxyl, and amino groups. The observations thus substantiate the existence of CMC on the surface of Cu-NPs.

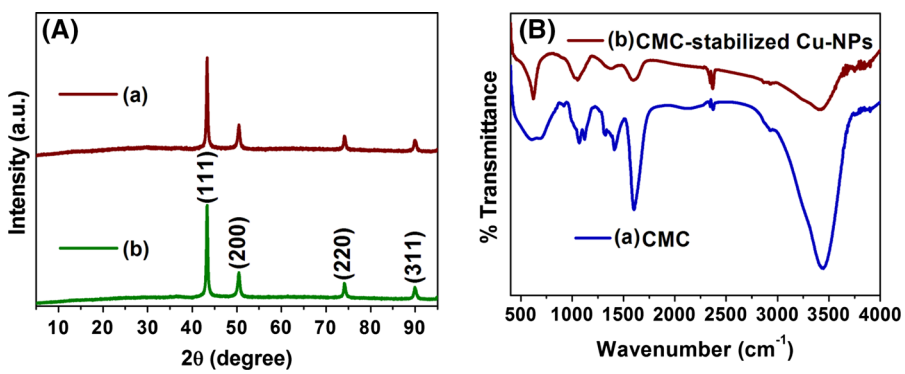

Fig. 2 **A** XRD patterns of CMC-stabilized Cu-NPs; (*a*) as synthesized (*b*) after 60 days. **B** FT-IR spectra of (*a*) CMC (*b*) CMC-stabilized Cu-NPs

Particle size analysis

Size and crystalline nature of CMC–Cu-NPs have been investigated through HRTEM and the corresponding micrographs have been presented in Fig. 3(A–C).The micrograph depicted in Figure 3A reveals the spherical shape of CMC–Cu-NPs with diameters in the range ~4–15 nm having ~1–2 nm (using ImageJ software) thin surface coating of the polymer, CMC. Size distribution of CMC–Cu-NPs has been given by the histogram shown in the inset of Fig. 3A; the histogram is obtained by analyzing a number of particles located in Fig. 3A using ImageJ software. Surface coating controls the aggregation and agglomeration tendencies of Cu-NPs resulting in the uniform distribution of CMC–Cu-NPs. High magnification micrograph depicted in Fig. 3B reveals the lattice fringes, and the fringe spacing between the adjacent lattice planes is found to be ~0.207 nm, which is in close agreement with the inter-planar distance of (111) planes of metallic Cu with FCC crystal structure ($d_{111} = 0.2087$ nm).

The selected area electron diffraction (SAED) pattern presented in Fig. 3C shows concentric ring pattern, characterizing the polycrystalline nature of the CMC–Cu-NPs. The d_{111}, d_{200}, d_{220}, and d_{311} values obtained for metallic Cu from XRD studies have been found to closely match with the *d*-spacing values calculated from the radii of the respective first four concentric rings observed in the SAED pattern, and thus they can be assigned to the (111), (200), (220), and (311) planes in the metallic Cu (JCPDS, File No. 04–0836).

Surface morphology analysis

Surface morphology of the synthesized powder of CMC-stabilized Cu-NPs has been obtained through FESEM and the corresponding image has been presented in Fig. 3D. The micrograph reveals the

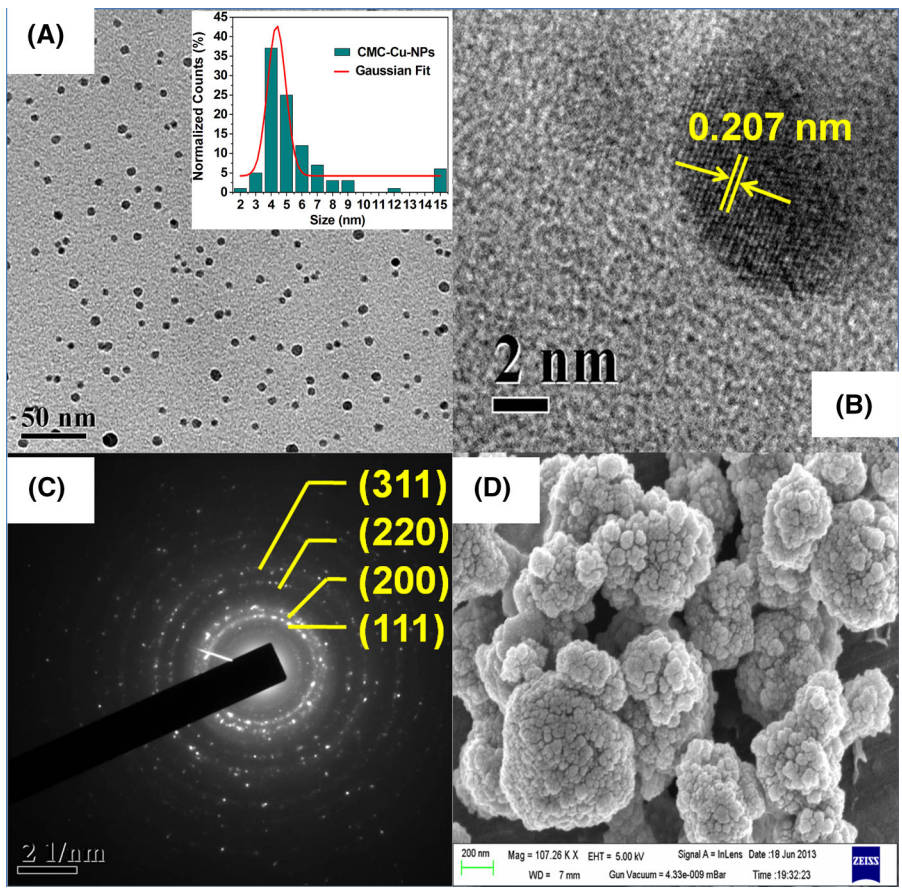

Fig. 3 **A** Bright Field HRTEM image of CMC-stabilized Cu-NPs (*Inset* shows nanoparticle size histogram); **B** High-resolution TEM image showing lattice fringes; **C** SAED pattern of CMC-stabilized Cu-NPs; **D** FESEM image of CMC-stabilized Cu-NPs

spherical morphology of the CMC–Cu-NPs with diameters in the range ~5–20 nm. The size of CMC–Cu-NPs has been calculated using ImageJ software through consideration of the smallest agglomerate as a single unit. Agglomeration of small NPs in its powder form in case of FESEM is probable cause behind the small inconsistency of diameters obtained from HRTEM and FESEM.

Thermal studies

Thermal properties of the CMC-stabilized Cu-NPs have been studied through thermogravimetric analysis (TGA), differential thermal analysis (DTA), and derivative of thermogram (DTG) analysis in Argon and Oxygen atmospheres, and they have been, respectively, depicted in Fig. 4A(a,b), B(a,b), C(a, b). Both in Argon and Oxygen atmospheres, CMC–Cu-NPs show a mass loss up to 127 °C possibly due to the evaporation of physically adsorbed water molecules. The DTA curve (Fig. 4B(a)) of CMC-Cu-NPs shows an exothermal effect between 130 and 700 °C in argon atmosphere, which has an associated total mass loss of ~6.2 % in the TGA curve (Fig. 4A(a)). The corresponding DTG curve as depicted in Fig. 4C(a) signifies 172 and 317 °C in which comparatively higher rate of mass loss happens. The thermal effect in argon atmosphere may be assigned to the multistep thermal degradation of surface attached CMC occurring via decarboxylation and decomposition of glucosamine units (Kittur et al. 2002; Ujang et al. 2011) of CMC. However, in oxygen atmosphere, the TGA curve (Fig. 4A(b)) shows a mass gain of ~15.4 % instead of mass loss in the same temperature range (i.e., ~130–700 °C). The corresponding DTG curve as presented in Fig. 4C(b) shows that higher rate of mass change happens at around 153, 204, 241, and 306 °C, while the associated DTA curve (Fig. 4B(b)) reveals a multistep exothermal effect that can probably be correlated to the combined effect of decomposition of CMC, oxidation of Cu, and combustion of any carbonaceous residue (from CMC). The mass gain in the same temperature range may be attributed to the oxidation of Cu-NPs in oxygen environment, which supersedes any mass loss effect associated with the degradation of CMC.

Zhang et al. have reported the appearance of three exothermic peaks (positioned at 233, 279, and 531 °C) in the SDTA (Scanning DTA) curve of pure Cu-NPs in oxygen atmosphere (Zhang et al. 2007), and they have associated those with surface oxidation of Cu_2O to CuO, oxidation of the cores of Cu-NPs to Cu_2O and oxidation of Cu_2O cores to CuO, respectively, where Cu was presumed to be converted to Cu_2O on the surface of the NPs through surface oxidation (oxidation of pure Cu-NPs takes place at ~134 °C). In comparison, the exothermic peaks in the DTA curve for CMC–Cu-NPs in oxygen atmosphere have been observed at ~158, 205, 243, and 304 °C which are correlated with DTG minima (as shown in Fig. 4C(b)). The exothermic peak at ~158 °C may be attributed to simultaneous thermal effect associated with degradation of CMC (mainly decarboxylation) and oxidation of Cu to Cu_2O. The observed peaks at ~205, 243, and 304 °C may, respectively, be compared with the three oxidation steps of Cu reported by Zhang et al. (2007). It may, however, be noted that exothermic peak temperatures observed for CMC–Cu-NPs are lower

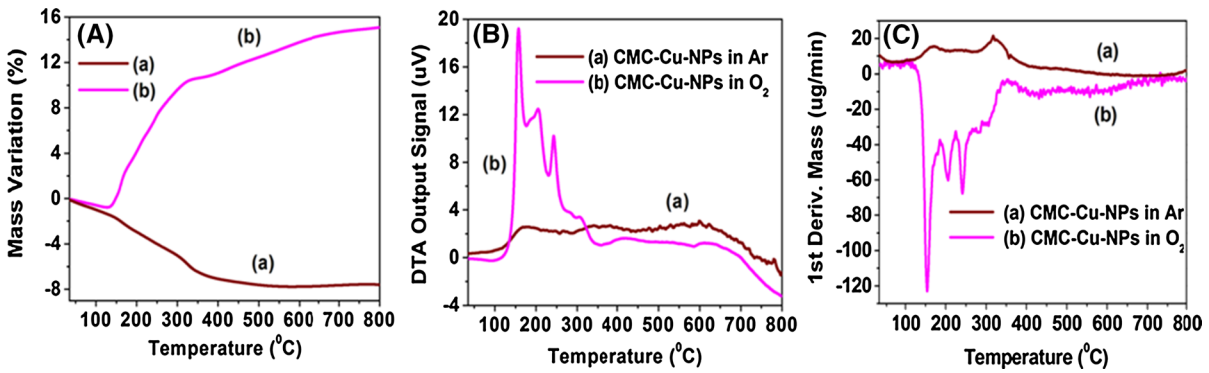

Fig. 4 **A** TGA, **B** DTA, and **C** DTG curves of CMC-stabilized Cu-NPs; (*a*) in the presence of Argon, (*b*) in the presence of Oxygen

than those reported for pure Cu-NPs by Zhang et al. (2007). This lowering in temperature may be due to the catalytic activity of Cu-NPs toward decomposition of CMC and oxidation/combustion of any carbonaceous residue (from CMC), and the heat generated in the process possibly facilitates the lowering of the external temperatures required for the oxidation of Cu. Moreover, it needs to be emphasized that the decomposition of CMC, oxidation of Cu, and combustion of carbonaceous residue from CMC all occur almost simultaneously, and it is difficult to assign any one effect to any one of the exotherms observed in DTA curve (Fig. 4B(b)).

Assuming complete oxidation of Cu-NPs to CuO at 800 °C, the Cu content in CMC–Cu-NPs sample is estimated to be ~92 %, and CMC, the stabilizing agent, mounts to ~6–8 % of the total sample's mass.

Dynamic light scattering (DLS) and zeta potential (ZP) measurements

The pH-dependent variation of effective hydrodynamic diameters (HDs) and zeta potentials (ZPs) of CMC-stabilized Cu-NPs have been studied and their respective plots have been shown in Fig. 5A(a, b). Positive ZP values signify a net positive surface charge on the CMC-stabilized Cu-NPs. In the acidic pH, the free $–NH_2$ groups from the CMC present on the surface of Cu-NPs are expected to get protonated and are likely to impart a net positive charge to the NP surface through generation of $–NH_3^+$ species. Likewise, deprotonation of the free –COOH groups (in CMC) in basic medium confers a net negative charge to the NP surface, via the formation of $–COO^-$ species, and hence result in negative values of ZP. The observed positive ZP values of CMC-stabilized Cu-NPs (shown in Fig. 5A(b)) in acidic pH (i.e., + 21.2 mV at pH = 3), its decrease to +7.2 mV with increase in pH to 8, and its eventual negative values in the basic medium (i.e., −14.1 mV at pH = 12) are thus consistent with protonation of amine with decrease in pH and successive deprotonation of the carboxyl groups associated with the increase in pH. The transition from positive to negative values of ZP (i.e., the isoelectric point) is found to occur in the pH = 8.7.

Figure 5A(a) reveals that the effective HD of the CMC-stabilized Cu-NP is 159.2 nm at pH = 3, which increases with increase in pH and reaches a maximum value of 222.2 nm at pH ~8 (i.e., near the isoelectric point). With the increase in pH beyond 8, the effective HD values are again found to decrease and reach a value of 131.9 nm at pH = 12. It may be deliberated that in both acidic and basic medium (i.e., pH below and above the isoelectric point respectively), the electrostatic repulsion between the similarly charged surfaces of the NPs probably prevents their aggregation/agglomeration and consequentially their effective HDs are observed to be lower. Conversely, with the increase in pH from 3 to 8, the positive charge developed on the NP surface due to the protonation of the amine groups (i.e., $–NH_3^+$) gets counterbalance by the negative charge generated due to successive deprotonation of the carboxyl groups (i.e., $–COO^-$) of CMC.

The electrostatic interaction between the positively and negatively charged surfaces possibly leads to coalesce of the NPs through intermolecular H-bonding

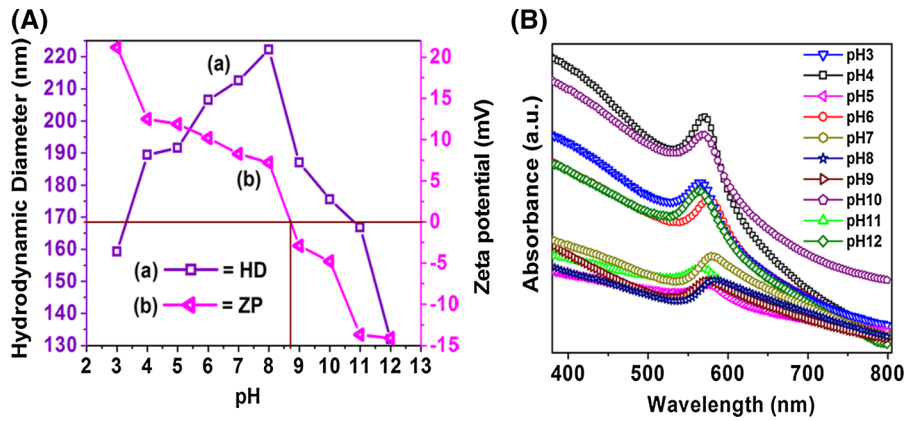

Fig. 5 Variation of **A**(*a*) hydrodynamic diameter, **A**(b) zeta potential, and **B** UV–Visible spectrum of CMC-stabilized Cu-NPs with pH

and thereby increases their effective HD values. The aqueous colloidal dispersion of CMC-stabilized Cu-NPs has been observed to be stable throughout the experimental pH range of 3–12, which encompasses the physiological pH range of 7.2–7.4, with the average polydispersity index (PDI) of 0.21. Individual PDI value obtained during DLS measurements in the above pH range (3–12) has been presented in Table S2 under the 'Supplementary Material 1', and 0.21 is the average of ten (10) PDI values.

Optical characterization

The UV–Vis absorption spectra of the colloidal dispersions of CMC-stabilized Cu-NPs, depicted in Fig. 5B, show the surface plasmon resonance (SPR) effect exhibited by Cu-NPs in the visible region (500–600 nm) of electromagnetic radiation. The strong absorption maxima (i.e., of the SPR bands), which occur due to resonance between the frequency of the electromagnetic field and the collective oscillation of the free conducting electrons (Ghosh and Pal 2007) of Cu-NPs, are the origin of the wine-red colors of the colloidal dispersions. Figure 5B shows that the λ_{max} of the SPR absorption band shifts with variation of pH from 3 to 12. It may be noted that the λ_{max} value at pH = 3 is 565 nm, which gets red-shift to 583 nm with increase in the pH up to 8. Increase of pH beyond 8, however, shows the corresponding λ_{max} values to be blue-shifted and eventually acquires a value of 563 nm at pH = 12. Hence there are red-shifts in the λ_{max} values on increase in pH from 3 to 8 and blue-shifts on further increase in pH from 8 to 12. This red-shift in the λ_{max} can be corroborated with the observed increase in the effective HDs of the CMC-stabilized Cu-NPs in the same pH range of 3–8 and the blue-shift to their decrease between the pH of 8–12. The observation is also in agreement with the reported literature (Ghosh and Pal 2007; Soomro et al. 2013) which states that the resonance wave length of SPR (λ_{max}) depends on the size, shape, dielectric medium, inter-particle interaction, and on the local chemical surroundings of the metal NPs.

It may thus be inferred that near the isoelectric point (pH = 8.7) when the particles tend to aggregate and agglomerate to result in the larger value of effective HD, their surface plasmons couple as the conduction electrons on each particle surface collectively oscillate. This results in the oscillating electrons assuming the lowest energy state, causing the plasmon resonance wavelength (λ_{max}) of the coupled particles to red-shift to longer wavelengths (i.e., 583 nm).

XPS analysis

X-ray photoelectron spectroscopy (XPS) analysis has been carried out to ascertain the chemical and oxidation states of copper in the CMC-stabilized Cu-NPs, and the respective survey spectrum showing signature for Cu, O, N, C, and Al (contamination) has been depicted in Fig. 6A. C 1 s (284.625 eV) has been used as reference to the obtained binding energy values from XPS. The de-convoluted and curve-fitted narrow spectra of Cu 2p, illustrated in Fig. 6B, show two strong peaks at 932.62 and 952.5 eV corresponding to the characteristic Cu $2p_{3/2}$ and Cu $2p_{1/2}$ photoelectron transitions (Chen et al. 2011; Jiang et al. 2014) of Cu^0, respectively. The spectra of Cu 2p do not show any satellite feature characteristic of Cu^{2+} species (usually expected to appear centered around 940–945 eV) thus, infers the absence of CuO in the sample (Rastogi and Arunachalam 2013). Similar binding energy values of Cu^+ and Cu^0 (around 932.6 eV) make it difficult to distinguish their existence through XPS. However, corroborating with the findings from XRD analysis, which show no sign of the presence of Cu_2O, the peak at 932.62 eV may be believed to arise only from Cu^0. Again, the line-shape and peak-to-peak separation between Cu $2p_{3/2}$ and Cu $2p_{1/2}$ of 19.88 eV are consistent with the reported data for elemental Cu (Rastogi and Arunachalam 2013). XPS narrow spectra (de-convoluted and curve-fitted) of C 1 s, O 1 s, and N 1 s have been presented in Fig. 6C–E, respectively. Two peaks in O 1 s (at 531.25 and 532.25 eV), a single peak in N 1 s (at 400.05 eV), and the corresponding four peaks in C 1 s (at 286.87, 288.5, 285.25, and 284.62 eV) are in good agreement with the respective reported binding energy values (Ahren et al. 2012; Sreedhar et al. 2007) of C–O, C=O, C–N, and C–C bonds, which substantiate their existence and may be associated with CMC in the CMC-stabilized Cu-NPs.

Formation of CMC-stabilized Cu-NPs

Cu(II) ions from copper sulfate pentahydrate interact with electron-rich CMC polymer to form a whitish blue colored complex (Cu^{2+}-CMC) through electrostatic

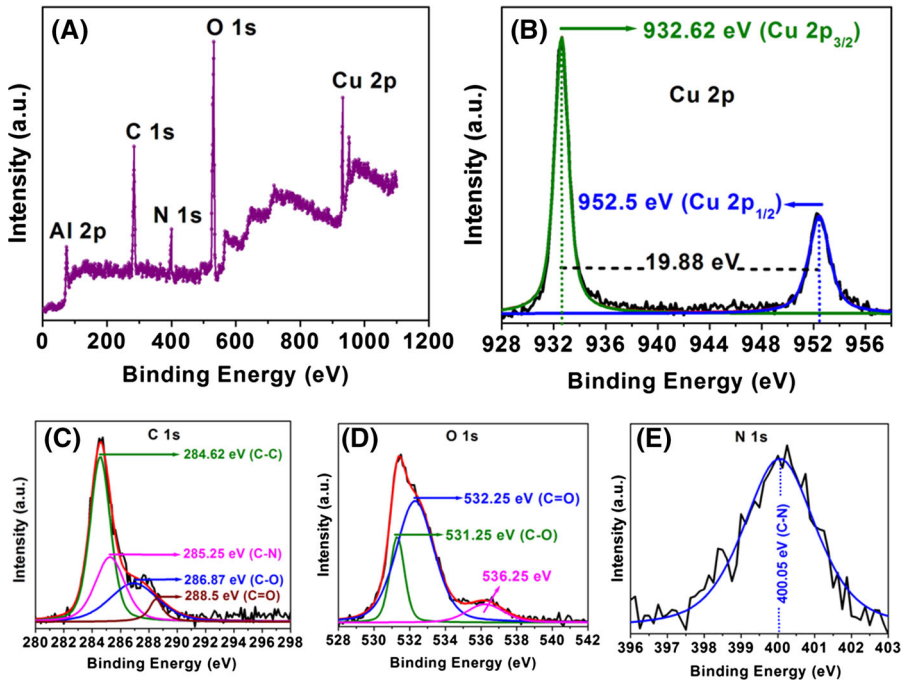

Fig. 6 XPS survey profile of CMC-stabilized Cu-NPs **A**; XPS *narrow* profile with de-convoluted and curve-fitted spectra of **B** Cu 2p, **C** C 1 s, **D** O 1 s, and **E** N 1 s of CMC-stabilized Cu-NPs

attraction (Sun and Wang 2006). Hydrazine reduces the Cu^{2+} ions in the complex to Cu^0 under microwave irradiation. pH of the reaction mixture is maintained at 9 to enhance the reducing ability of hydrazine.

Based on the findings from the XRD, IR, and UV–Vis studies, the possible mechanism for the formation of CMC-stabilized Cu-NPs can be given as follows:

$$CU^{2+} + CMC \rightarrow [Cu\ (CMC)]^{2+} \quad (1)$$

$$2[Cu(CMC)]^{2+} + N_2H_4 + 4OH^- \rightarrow 2[Cu\ (CMC)]^0 + N_2 + 4H_2O. \quad (2)$$

Hydrazine reduces the copper ions instantaneously, thereby diminishing the possibility of the formation of impurity oxide phase [such as Cu_2O and $Cu(OH)_2$]. Further, continuous release of N_2 during the reduction process provides an inert atmosphere in situ and thus avoids the need of any external source of inert gas during the synthesis. The procedure has good reproducibility for which it can be used for large-scale synthesis of Cu-NPs. Moreover, the CMC acts as a surface coating and stabilizing agent that helps to retain stability of the aqueous dispersion of Cu^0 up to 2 months. In has been further observed that the stability of the dispersion can be prolonged for 5–6 months with the addition of ascorbic acid during the synthesis.

Antimicrobial properties

As shown in Fig. 7, CMC-stabilized Cu-NPs showed significant inhibitive zones against tested pathogens, *C. tropicalis* (Fig. 7A) and *E. coli* (Fig. 7B) in comparison to $CuSO_4 5H_2O$ (control 1) and CMC (control 2) through agar well diffusion method. The Antimicrobial activity of CMC-stabilized Cu-NPs against pathogens was further determined by broth dilution method. Microbial growth inhibition was observed for the cells incubated with CMC-stabilized Cu-NPs at 3.9 to −0.24 μg mL^{-1} for 16 h in dose dependent manner, as validated by CLSI-broth dilution data given in Fig. 7C. The growth inhibition of *C. tropicalis* and *E. coli* was found to be significant (~50 % growth inhibition at 1.95 and 0.24 μg mL^{-1}, respectively) in the presence of CMC-stabilized Cu-NPs. The antibacterial activity of CMC-stabilized Cu-NPs is stronger than most of the previous reports (see Table S1 under 'Supplementary Material 1' for comparison with other antimicrobial Cu-NPs/Nanocomposites, copper salts, and commercially available antibiotics) on antimicrobial Cu-NPs (Raffi et al. 2010; Ruparelia et al. 2008). Moreover, the potent antifungal activity CMC-stabilized Cu-NPs on *C. tropicalis* enhances the necessity of the present work, as there is no such report with Cu-NPs till now

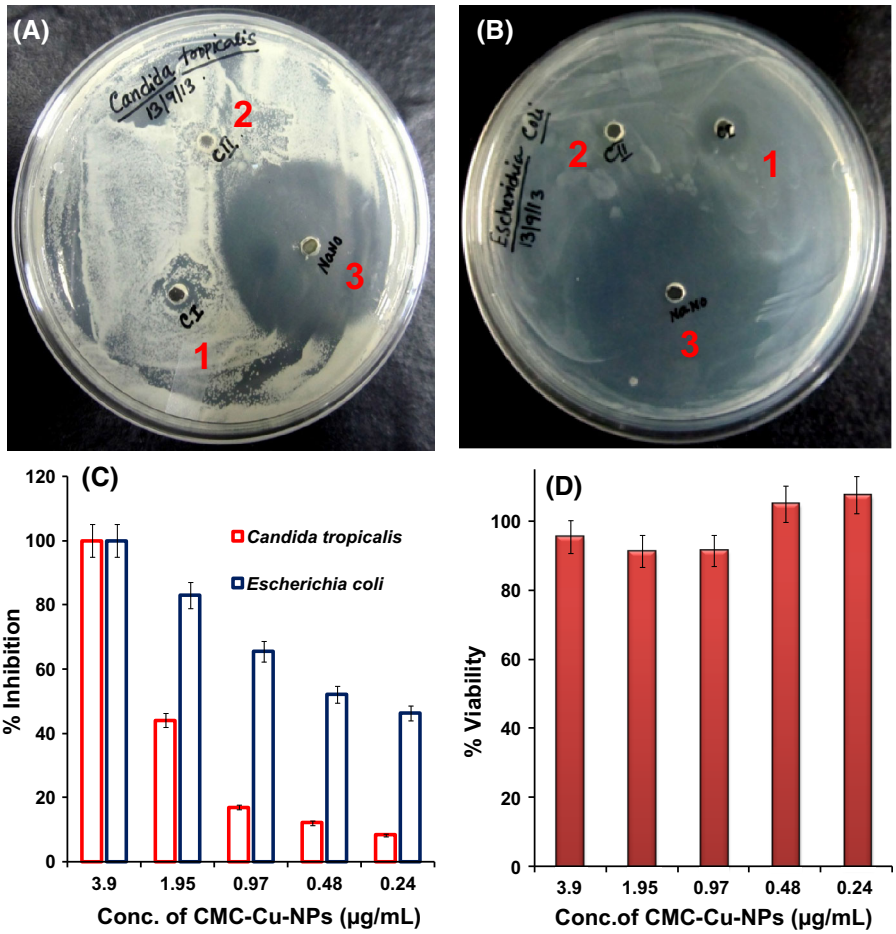

Fig. 7 Antimicrobial screening by agar well diffusion method for **A** *Candida tropicalis* (NCIM 3110) and **B** *Escherichia coli* (ATCC 25922) using 1, C1: $CuSO_4 5H_2O$; 2, CII: CMC; and 3, Nano: CMC-stabilized Cu-NPs. **C** Dose-dependent antimicrobial activity of CMC-stabilized Cu-NPs, obtained through monitoring the microbial growth (measured at 600 nm after incubation for 16 h at 37 ± 2 °C) at different concentrations of CMC-stabilized Cu-NPs studied by CLSI broth dilution method for *Candida tropicalis* (NCIM 3110) (*Red*) and *Escherichia coli* (ATCC 25922) (*Blue*). Data are the mean of triplicate experiments ± S.E; **D** % of cell viability of L929 cells after treatment with CMC-stabilized Cu-NPs, as measured by MTT assay. (Color figure online)

(as per the best of authors' knowledge), though fungicidal effect of Cu-NPs on *C. albicans* is not new (Usman et al. 2013).

The viability of microbes upon treatment with CMC-stabilized Cu-NPs was also assessed through LIVE/DEAD viability assay, where live cells having intact cell membranes fluoresce green due to the staining with SYTO 9, and dead cells with damaged membranes fluoresce red due to the staining with propidium iodide (PI).The results of this study indicate that viability of cells decreases upon treatment with CMC-stabilized Cu-NPs in comparison to the control cells (Figs. 8, 9).

NPs for antimicrobial therapy should be absorbable to cells with sufficiently high rate of extent. Previously, it has been proposed that the size of the particles plays a key role in their adhesion and interaction to biological cells. NPs with a larger surface-to-volume ratio provide more efficient means of antimicrobial activity (Raffi et al. 2010). In the present study, the promising antimicrobial activity of CMC-stabilized Cu-NPs may be due to its small size (4–15 nm).

It has been reported that the interaction between cationic charged NPs with negatively charged bacterial cell membrane occurred by electrostatic interaction or adsorption (De et al. 2010). The overall positive

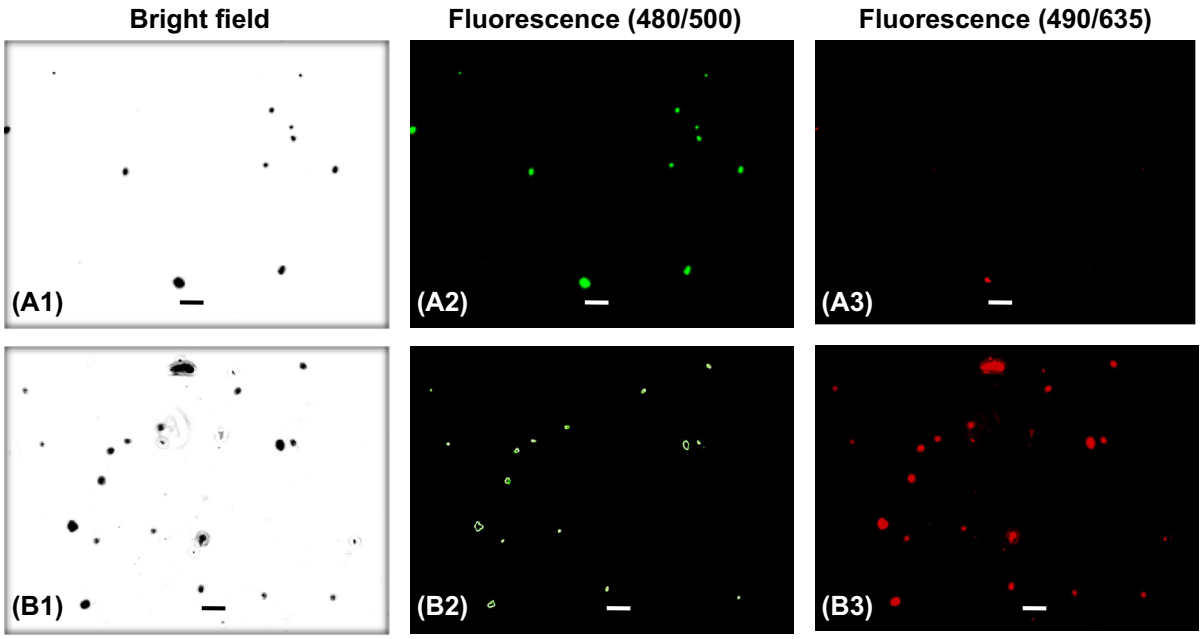

Fig. 8 Fluorescence microscopy images for live/dead viability assay carried out on *Candida tropicalis* (NCIM 3110) for (*A1*, *A2*, *A3*) Control; (*B1*, *B2*, *B3*) on treatment with CMC-stabilized Cu-NPs [*Color* index: *Green* = live cell; *Red* = dead cell; *Green* + *red* = dead cell]. Imaging was done using fluorescence microscope (IX 51, Olympus) with high-performance CCD camera and Image-Pro discovery 5.1 software. *Scale bar* = 10 μm. (Color figure online)

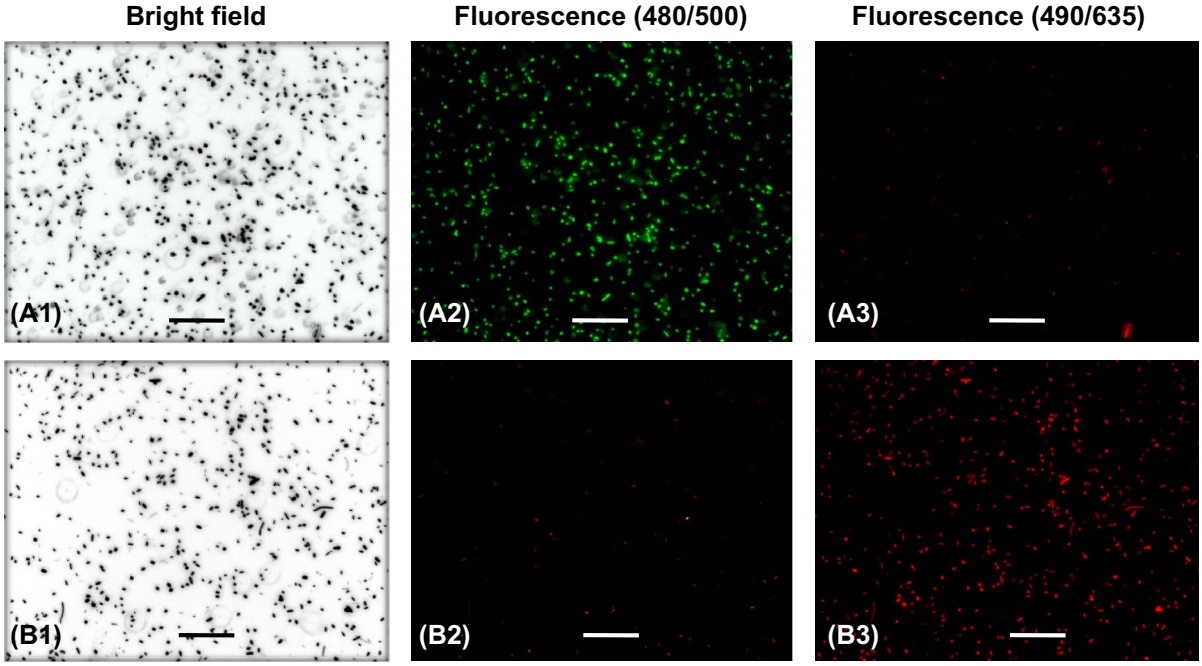

Fig. 9 Fluorescence microscopy images for live/dead viability assay carried out on *Escherichia coli* (ATCC 25922) (*A1*, *A2*, *A3*) for control; (*B1*, *B2*, *B3*) on treatment with CMC-stabilized Cu-NPs [*Color* index: *Green* = live cell; *Red* = dead cell; *Green* + *red* = dead cell]. Imaging was done using fluorescence microscope (IX 51, Olympus) with high-performance CCD camera and Image-Pro discovery 5.1 software. *Scale bar* = 10 μm. (Color figure online)

charge of $\sim +8.3$ mV of the presently synthesized CMC-stabilized Cu-NPs implies that they might bind to cell membranes and cause membrane destruction.

Microscopic observation

Electron microscopy and Atomic force microscopy are widely used to image the morphology and surface topography of cells at high resolution (Ahimou et al. 2003). Microbial cell destruction in effect of CMC-stabilized Cu-NPs has been shown by field emission scanning electron microscopic (FESEM) (Figs. 10, 11) and atomic force microscopic (AFM) (Fig. 12) images. The mechanism by which NPs are able to affect microbial cells is not understood completely, but studies reveal that when microbial cells are treated with Cu-NPs, changes take place in its cell surface.

FESEM micrographs of *C. tropicalis* and *E. coli* (control and treated with CMC-stabilized Cu-NPs in both the cases) (Figs. 10, 11) show about the cell transformation from normal shape to an irregular appearance after treatment with CMC-stabilized Cu-NPs. Some cells are discovered even to have shrunk and cell wall is found destroyed and uneven. Figure 10 represents the morphology of CMC-stabilized Cu-NPs-treated fungal cells where fungal cell destruction (Fig. 10D, E) and cell wall disorganization (Fig. 10F) are observed as compared to control cells (Fig. 10A–C). Similarly, Fig. 11 shows the FESEM images of bacteria treated with CMC-stabilized Cu-NPs, in which NPs are found to be adhered to the bacterial cell surface (Fig. 11F) and resulted in bacterial cell membrane destruction and cell lysis (Fig. 11D, E) as compared to control cells (Fig. 11A–C).

Atomic force microscopy (AFM) was used to image the surface topography of cells. The surface of native cells image is homogeneous and smooth (Fig. 12A, C). As shown in Fig. 12A–D RMS heights (RMS height is defined as square root of the average of the squares of all the heights of the irregularities w.r.t. a reference line, and this measures surface roughness. In the present study, RMS heights have been obtained from AFM images using Pico image basic software) of fungus and bacteria decrease from 415 nm (Fig. 12A) and 86.1 nm (Fig. 12C) to 26.7 nm (Fig. 12B) and 68.7 nm (Fig. 12D), respectively, thereupon

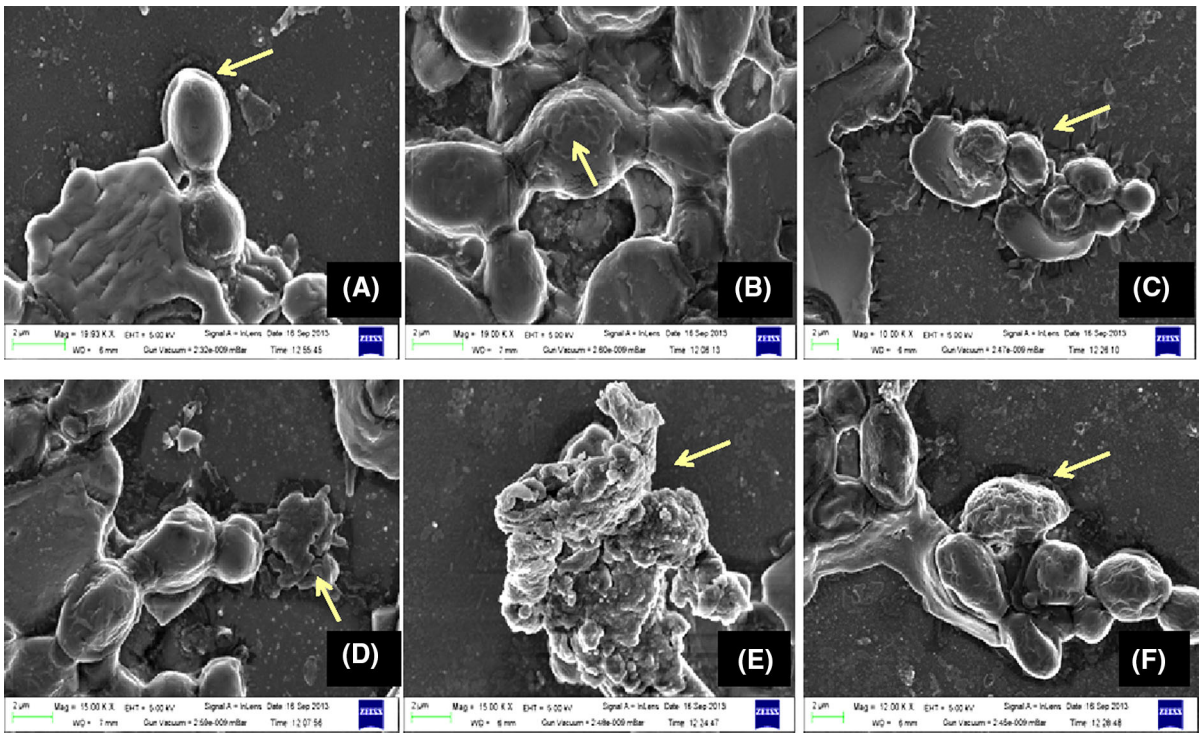

Fig. 10 FESEM Micrographs of *Candida tropicalis* (NCIM 3110) for three controls (**A**), (**B**), and (**C**); and respective images on treatment with CMC-stabilized Cu-NPs (**D**), (**E**), and (**F**)

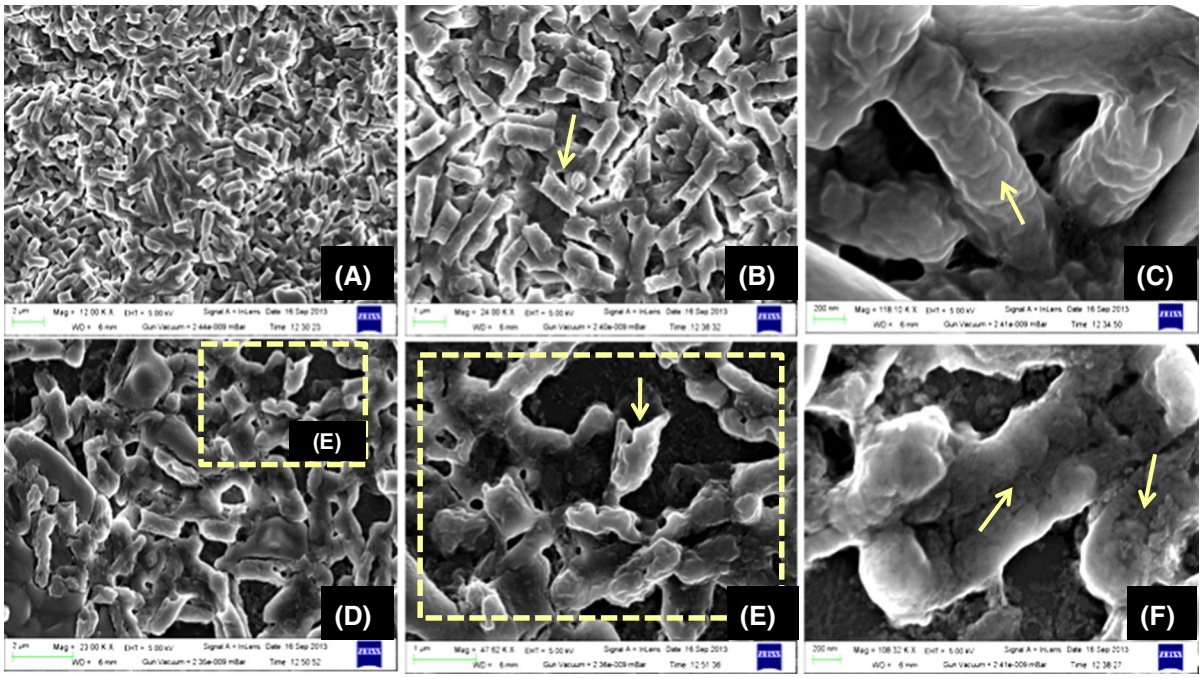

Fig. 11 FESEM micrographs of *Escherichia coli* (ATCC 25922) for three controls (**A**), (**B**), and (**C**); and the respective images on treatment with CMC-stabilized Cu-NPs (**D**), (**E**), and (**F**)

indicating microbial cell shrinkage due to fluid loss as an effect from CMC-stabilized Cu-NPs.

CMC affects the antimicrobial activity of Cu-NPs through various ways, such as CMC may provide strong bridging between cell membranes of microbes and Cu-NPs resulting higher microbial activity (Goy et al. 2009); besides, surface stabilization with CMC decreases aggregation/agglomeration tendency of Cu-NPs, ensuing increase of the effective concentration of Cu-NPs having interacting capability with microbial surface. Upon binding, an efflux of nutrients is believed to occur between the cell wall and the cell membrane, which enlarges, and the cytoplasm tends to concentrate. Mallick et al. have reported that antibacterial activity of Cu-NPs is related with the attachment of Cu-NPs to the cell wall causing leakage of proteins in addition to other intracellular materials, which finally cause cell death (Mallick et al. 2012). Several studies describe that antimicrobial activity of copper and copper-containing compounds such as $CuSO_4$ and $Cu(OH)_2$ in aqueous medium is associated with release of copper ions (Anyaogu et al. 2008; Cioffi et al. 2005; Hughes and Poole 1989) having the capacity to kill microbes by destroying their cell walls and membranes due to their strong reduction ability (Raffi et al. 2010). Again some groups have reported that filamentous cell growth and reactive oxygen species (ROS) induced DNA damage and membrane ruptures may also occur in the presence of antibacterial Cu(0)/Cu(I)-NPs (Chatterjee et al. 2012; Pramanik et al. 2012). However, no work has been done in molecular detail to understand the exact mechanism of action. At present, there are debates regarding the mechanism of chemical action of metallic NPs—whether the NPs themselves or the ions released from them are responsible for antimicrobial action of NPs. If the mere ions are responsible, the prime ingredient (here $CuSO_4{\cdot}5H_2O$) will be equally potent to kill the microbes; it is not the case; the prime ingredient shows very less antimicrobial activity toward *C. tropicalis* and *E. coli* (agar well diffusion study indicates that zones of inhibitions for $CuSO_4{\cdot}5H_2O$ having nearly equivalent amount of Cu^{2+} as present in CMC-stabilized Cu-NPs are very small compared with that for NPs). For this, nascent Cu ions (Chatterjee et al. 2014) liberated from the NPs surface may be responsible for higher activity of the Cu-NPs than the equivalent amount of its precursor $CuSO_4{\cdot}5H_2O$. The

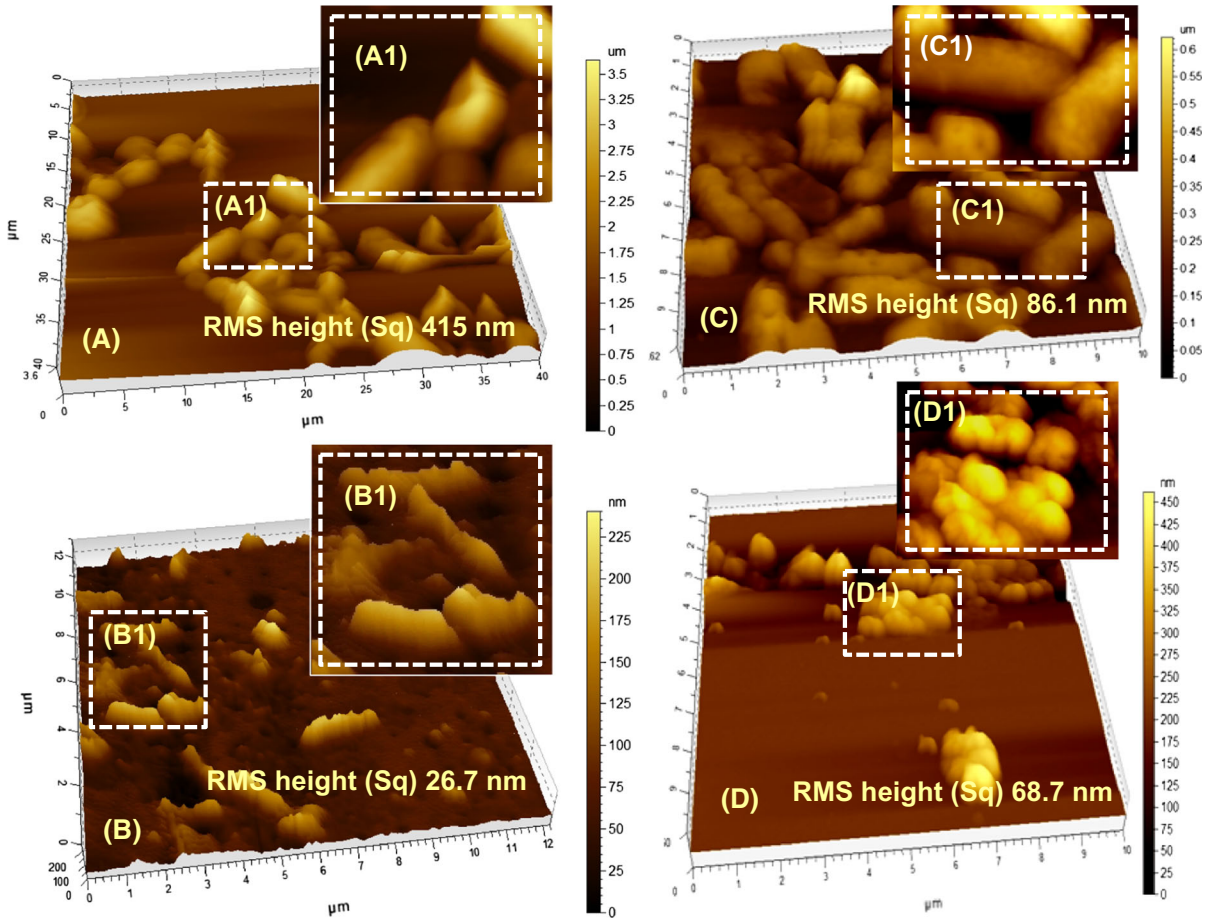

Fig. 12 AFM images of *Candida tropicalis* (NCIM 3110) **A** control, **B** on treatment with CMC-stabilized Cu-NPs; and of *Escherichia coli* (ATCC 25922) **C** control, **D** on treatment with CMC-stabilized Cu-NPs

mechanism of antimicrobial action of CMC-stabilized Cu-NPs has not been deduced yet, further study is required. However, the present investigation might provide modest insight into the complicated antimicrobial action of CMC-stabilized Cu-NPs.

Cytotoxicity assay

Toxicity of free Cu to mammalian cells is well known, and exposure to Cu in the form of NPs brings additional concerns over potential health effects. As smaller-sized Cu-NPs may cause more toxicity than larger-sized Cu-NPs (Prabhu et al. 2010), the cytotoxic effects of such significantly small CMC-stabilized Cu-NPs (diameters ~4–15 nm) on normal cells must be evaluated before use as an antimicrobial agent for practical purposes. Cytotoxicity of CMC-stabilized Cu-NPs in vitro was determined by conventional MTT assay using normal cell line, L929 (See Section 3 of 'Supplementary Material 1' for experimental details). The effects of CMC-stabilized Cu-NPs on cell growth have been shown in Fig. 7D. It is found that CMC-stabilized Cu-NPs have no significant toxicity to normal cells at the concentration of 3.9 µg/mL (Cell viability ~95 %), in which it exhibit potent antimicrobial activity. Hence, potential health risks of CMC-stabilized Cu-NPs have been minimized, and it may be used in medical applications.

Conclusions

In conclusion, a simple and time-efficient solution-based method has been developed for the preparation of

CMC-stabilized copper nanoparticles (Cu-NPs) through microwave irradiation-assisted reduction of copper(II)–CMC complex by hydrazine in aqueous medium and under ambient atmosphere. Surface coating with the biocompatible polymer, CMC, not only prevented the surface oxidation of the NPs of pure metallic Cu but also restricted their diameters within 4–15 nm to facilitate their homogenous dispersion in aqueous medium that remained stable for more than 2 months without any sign of sedimentation when retained in air-tight container and in the pH range of 3–12. The spherical, CMC-stabilized Cu-NPs exhibited very good antimicrobial activity against fungal (*C. tropicalis*) (NCIM 3110) and bacterial (*E. coli*) (ATCC 25922) pathogens, which is significant than most of the antimicrobial Cu-NPs reported earlier. Besides, the additional concerns over the potential health risks associated with Cu-NPs have been reduced for the synthesized antimicrobial agent, as CMC-stabilized Cu-NPs showed considerably lower-toxicity to normal cells. Antimicrobial activity of these spherical, positively charged ($\sim +8.3$ mV) Cu-NPs in neutral pH is attributed to their ability to trigger off cell death when they may get attached to the negatively charged microbial cells and cause irreversible damage to their cell membrane. Leakage of intracellular metabolites and fluid loss from the damaged microbial cell membrane eventually culminate the cell death. The developed antimicrobial agent may be explored as an alternative of antibiotics, and it may also have the potential to utilize in sterilization of hospital equipment, wound dressing, waste-water treatment etc.

Acknowledgments The authors would like to acknowledge the DST-FIST funded XPS facility at the Department of Physics and Meteorology, IIT Kharagpur. The authors would also like to acknowledge Prof. Nilmoni Sarkar, Department of Chemistry for his kind help. S.Tantubay is thankful to the University Grants Commission, New Delhi (Govt. of India) for providing fellowship.

Conflict of interest The authors declare no conflict of interest.

References

Ahimou FO, Touhami A, Dufrene YF (2003) Real-time imaging of the surface topography of living yeast cells by atomic force microscopy. Yeast 20:25–30. doi:10.1002/Yea.923

Ahren M et al (2012) A simple polyol-free synthesis route to Gd_2O_3 nanoparticles for MRI applications: an experimental and theoretical study. J Nanopart Res. doi:10.1007/S11051-012-1006-2

Anyaogu KC, Fedorov AV, Neckers DC (2008) Synthesis, characterization, and antifouling potential of functionalized copper nanoparticles. Langmuir 24:4340–4346. doi:10.1021/La800102f

Azocar MI et al (2014) A systematic study of antibacterial silver nanoparticles: efficiency, enhanced permeability, and cytotoxic effects. J Nanopart Res. doi:10.1007/S11051-014-2465-4

Basumallick S, Rajasekaran P, Tetard L, Santra S (2014) Hydrothermally derived water-dispersible mixed valence copper-chitosan nanocomposite as exceptionally potent antimicrobial agent. J Nanopart Res. doi:10.1007/s11051-014-2675-9

Bolshakova AV, Kiselyova OI, Yaminsky IV (2004) Microbial surfaces investigated using atomic force microscopy. Biotechnol Prog 20:1615–1622. doi:10.1021/Bp049742c

Chatterjee AK, Sarkar RK, Chattopadhyay AP, Aich P, Chakraborty R, Basu T (2012) A simple robust method for synthesis of metallic copper nanoparticles of high antibacterial potency against *E. coli*. Nanotechnology. doi:10.1088/0957-4484/23/8/085103

Chatterjee AK, Chakraborty R, Basu T (2014) Mechanism of antibacterial activity of copper nanoparticles. Nanotechnology. doi:10.1088/0957-4484/25/13/135101

Chen XG, Park HJ (2003) Chemical characteristics of O-carboxymethyl chitosans related to the preparation conditions. Carbohydr Polym 53:355–359. doi:10.1016/S0144-8617(03)00051-1

Chen SS et al (2011) Oxidation resistance of graphene-coated Cu and Cu/Ni alloy. ACS Nano 5:1321–1327. doi:10.1021/Nn103028d

Chudasama B, Vala AK, Andhariya N, Mehta RV, Upadhyay RV (2010) Highly bacterial resistant silver nanoparticles: synthesis and antibacterial activities. J Nanopart Res 12:1677–1685. doi:10.1007/s11051-009-9845-1

Cioffi N et al (2004) Antifungal activity of polymer-based copper nanocomposite coatings. Appl Phys Lett 85:2417–2419. doi:10.1063/1.1794381

Cioffi N et al (2005) Copper nanoparticle/polymer composites with antifungal and bacteriostatic properties. Chem Mater 17:5255–5262. doi:10.1021/Cm0505244

Clinical and Laboratory Standards Institute (2007). Performance standards for antimicrobial susceptibility testing; seventeenth informational supplement. CLSI Document. Wayne, Pennsylvania, USA. 27: M100-S117

De D, Mandal SM, Gauri SS, Bhattacharya R, Ram S, Roy SK (2010) Antibacterial effect of lanthanum calcium manganate (La0.67Ca0.33MnO3) nanoparticles against pseudomonas aeruginosa ATCC 27853. J Biomed Nanotechnol 6:138–144. doi:10.1166/jbn.2010.1113

Deng D, Jin Y, Cheng Y, Qi T, Xiao F (2013) Copper nanoparticles: aqueous phase synthesis and conductive films fabrication at low sintering temperature. ACS Appl Mater Interfaces 5:3839–3846. doi:10.1021/am400480k

Ferrer MCC, Hickok NJ, Eckmann DM, Composto RJ (2012) Antibacterial biomimetic hybrid films. Soft Matter 8:2423–2431. doi:10.1039/C2sm06969e

Ge HC, Luo DK (2005) Preparation of carboxymethyl chitosan in aqueous solution under microwave irradiation.

Carbohydr Res 340:1351–1356. doi:10.1016/j.carres.2005.02.025

Ghosh SK, Pal T (2007) Interparticle coupling effect on the surface plasmon resonance of gold nanoparticles: from theory to applications. Chem Rev 107:4797–4862. doi:10.1021/Cr0680282

Giuffrida S, Costanzo LL, Ventimiglia G, Bongiorno C (2008) Photochemical synthesis of copper nanoparticles incorporated in poly(vinyl pyrrolidone). J Nanopart Res 10:1183–1192. doi:10.1007/s11051-007-9343-2

Goy RC, de Britto D, Assis OBG (2009) A review of the antimicrobial activity of chitosan. Polimeros 19:241–247

Gu CJ, Sun B, Wu WH, Wang FC, Zhu MF (2007) Synthesis, characterization of copper-loaded carboxymethyl-chitosan nanoparticles with effective antibacterial activity. Macromol Symp 254:160–166. doi:10.1002/masy.200750825

Hughes MN, Poole RK (1989) Metals and micro-organisms. Chapman and Hall, London

Jain J, Arora S, Rajwade JM, Omray P, Khandelwal S, Paknikar KM (2009) Silver nanoparticles in therapeutics: development of an antimicrobial gel formulation for topical use. Mol Pharmaceut 6:1388–1401. doi:10.1021/Mp900056g

Jia BQ, Mei Y, Cheng L, Zhou JP, Zhang LN (2012) Preparation of copper nanoparticles coated cellulose films with antibacterial properties through one-step reduction. Acs Appl Mater Interaces 4:2897–2902. doi:10.1021/Am3007609

Jiang D et al (2014) Enhanced non-enzymatic glucose sensing based on copper nanoparticles decorated nitrogen-doped graphene. Biosens Bioelectron 54:273–278. doi:10.1016/j.bios.2013.11.005

Kahrilas GA et al (2014) Investigation of antibacterial activity by silver nanoparticles prepared by microwave-assisted green syntheses with soluble starch, dextrose, and arabinose. Acs Sustain Chem Eng 2:590–598. doi:10.1021/Sc400487x

Kittur FS, Prashanth KVH, Sankar KU, Tharanathan RN (2002) Characterization of chitin, chitosan and their carboxymethyl derivatives by differential scanning calorimetry. Carbohydr Polym 49:185–193. doi:10.1016/S0144-8617(01)00320-4

Kyriacou SV, Brownlow WJ, Xu XHN (2004) Using nanoparticle optics assay for direct observation of the function of antimicrobial agents in single live bacterial cells. Biochemistry 43:140–147. doi:10.1021/Bi0351110

Laudenslager MJ, Schiffman JD, Schauer CL (2008) Carboxymethyl chitosan as a matrix material for platinum, gold, and silver nanoparticles. Biomacromolecules 9:2682–2685. doi:10.1021/Bm800835e

Mallick S, Sharma S, Banerjee M, Ghosh SS, Chattopadhyay A, Paul A (2012) Iodine-stabilized Cu nanoparticle chitosan composite for antibacterial applications. Acs Appl Mater Interfaces 4:1313–1323. doi:10.1021/Am201586w

Martinez-Castanon GA, Nino-Martinez N, Martinez-Gutierrez F, Martinez-Mendoza JR, Ruiz F (2008) Synthesis and antibacterial activity of silver nanoparticles with different sizes. J Nanopart Res 10:1343–1348. doi:10.1007/s11051-008-9428-6

Moreno-Alvarez SA, Martinez-Castanon GA, Nino-Martinez N, Reyes-Macias JF, Patino-Marin N, Loyola-Rodriguez JP, Ruiz F (2010) Preparation and bactericide activity of gallic acid stabilized gold nanoparticles. J Nanopart Res 12:2741–2746. doi:10.1007/s11051-010-0060-x

Mott D, Galkowski J, Wang LY, Luo J, Zhong CJ (2007) Synthesis of size-controlled and shaped copper nanoparticles. Langmuir 23:5740–5745. doi:10.1021/La0635092

Mourya VK, Inamdar NN, Tiwari A (2010) Carboxymethyl chitosan and its applications. Adv Mat Lett 1:11–33

Panacek A et al (2006) Silver colloid nanoparticles: synthesis, characterization, and their antibacterial activity. J Phys Chem B 110:16248–16253. doi:10.1021/Jp063826h

Panacek A et al (2009) Antifungal activity of silver nanoparticles against *Candida* spp. Biomaterials 30:6333–6340. doi:10.1016/j.biomaterials.2009.07.065

Perez C, Paul M, Bazerque P (1990) An antibiotic assay by the agar well diffusion method. Acta Bio Med Exp 15:113–115

Powderly WG, Mayer KH, Perfect JR (1999) Diagnosis and treatment of oropharyngeal candidiasis in patients infected with HIV: a critical reassessment. AIDS Res Hum Retrovir 15:1405–1412. doi:10.1089/088922299309900

Prabaharan M, Gong S (2008) Novel thiolated carboxymethyl chitosan-g-beta-cyclodextrin as mucoadhesive hydrophobic drug delivery carriers. Carbohyd Polym 73:117–125. doi:10.1016/j.carbpol.2007.11.005

Prabhu BM, Ali SF, Murdock RC, Hussain SM, Srivatsan M (2010) Copper nanoparticles exert size and concentration dependent toxicity on somatosensory neurons of rat. Nanotoxicology 4:150–160. doi:10.3109/17435390903337693

Pramanik A, Laha D, Bhattacharya D, Pramanik P, Karmakar P (2012) A novel study of antibacterial activity of copper iodide nanoparticle mediated by DNA and membrane damage. Colloid Surf B 96:50–55. doi:10.1016/j.colsurfb.2012.03.021

Pulkkinen P, Shan J, Leppanen K, Kansakoski A, Laiho A, Jarn M, Tenhu H (2009) Poly(ethylene imine) and tetraethylenepentamine as protecting agents for metallic copper nanoparticles. Acs Appl Mater Interfaces 1:519–525. doi:10.1021/Am800177d

Raffi M, Mehrwan S, Bhatti TM, Akhter JI, Hameed A, Yawar W, ul Hasan MM (2010) Investigations into the antibacterial behavior of copper nanoparticles against *Escherichia coli*. Ann Microbiol 60:75–80. doi:10.1007/s13213-010-0015-6

Rastogi L, Arunachalam J (2013) Synthesis and characterization of bovine serum albumin-copper nanocomposites for antibacterial applications. Colloid Surf B 108:134–141. doi:10.1016/j.colsurfb.2013.02.031

Rippon JW (1988) Medical mycology: the pathogenic fungi and the pathogenic actinomycetes. Saunders, Philadelphia

Ruparelia JP, Chatteriee AK, Duttagupta SP, Mukherji S (2008) Strain specificity in antimicrobial activity of silver and copper nanoparticles. Acta Biomater 4:707–716. doi:10.1016/j.actbio.2007.11.006

Sarkar A, Mukherjee T, Kapoor S (2008) PVP-stabilized copper nanoparticles: a reusable catalyst for “Click” reaction between terminal alkynes and azides in nonaqueous solvents. J Phys Chem C 112:3334–3340. doi:10.1021/Jp077603i

Song XY, Sun SX, Zhang WM, Yin ZL (2004) A method for the synthesis of spherical copper nanoparticles in the organic phase. J Colloid Interfaces Sci 273:463–469. doi:10.1016/j.jcis.2004.01.019

Song J, Kang H, Lee C, Hwang SH, Jang J (2012) Aqueous synthesis of silver nanoparticle embedded cationic polymer nanofibers and their antibacterial activity. Acs Appl Mater Interfaces 4:460–465. doi:10.1021/Am201563t

Soomro RA et al. (2013) Synthesis of air stable copper nanoparticles and their use in catalysis. Adv Mat Let 1–23

Sreedhar B, Aparna Y, Sairam M, Hebalkar N (2007) Preparation and characterization of HAP/carboxymethyl chitosan nanocomposites. J Appl Polym Sci 105:928–934. doi:10.1002/App.26140

Sun SL, Wang AQ (2006) Adsorption kinetics of Cu(II) ions using N, O-carboxymethyl-chitosan. J Hazard Mater 131:103–111. doi:10.1016/j.jhazmat.2005.09.012

Usman MS, El Zowalaty ME, Shameli K, Zainuddin N, Salama M, Ibrahim NA (2013) Synthesis, characterization, and antimicrobial properties of copper nanoparticles. Int J Nanomed 8:4467–4478. doi:10.2147/Ijn.S50837

Ujang Z, Diah M, Rashid AHA, Halim AS (2011) The development, characterization and application of water soluble chitosan. Biotechnol Biopolym. doi:10.5772/16771

Valodkar M, Rathore PS, Jadeja RN, Thounaojam M, Devkar RV, Thakore S (2012) Cytotoxicity evaluation and antimicrobial studies of starch capped water soluble copper nanoparticles. J Hazard Mater 201:244–249. doi:10.1016/j.jhazmat.2011.11.077

Wang YF, Asefa T (2010) Poly(allylamine)-stabilized colloidal copper nanoparticles: synthesis, morphology, and their surface-enhanced raman scattering properties. Langmuir 26:7469–7474. doi:10.1021/La904199f

Wei YH, Chen S, Kowalczyk B, Huda S, Gray TP, Grzybowski BA (2010) Synthesis of stable, low-dispersity copper nanoparticles and nanorods and their antifungal and catalytic properties. J Phys Chem C 114:15612–15616. doi:10.1021/Jp1055683

Wu SH, Chen DH (2004) Synthesis of high-concentration Cu nanoparticles in aqueous CTAB solutions. J Colloid Interfaces Sci 273:165–169. doi:10.1016/j.jcis.2004.01.071

Zhang XF, Dong XL, Huang H, Wang DK, Lei JP (2007) High permittivity from defective carbon-coated Cu nanocapsules. Nanotechnology. doi:10.1088/0957-4484/18/27/275701

Zhang W, Shen H, Xie MQ, Zhuang L, Deng YY, Hu SL, Lin YY (2008) Synthesis of carboxymethyl-chitosan-bound magnetic nanoparticles by the spraying co-precipitation method. Scr Mater 59:211–214. doi:10.1016/j.scriptamat.2008.03.006

Zhang Y et al (2014) Facile preparation of monodisperse, impurity-free, and antioxidation copper nanoparticles on a large scale for application in conductive ink. Acs Appl Mater Interfaces 6:560–567. doi:10.1021/Am404620y

Zhao YY, Tian Y, Cui Y, Liu WW, Ma WS, Jiang XY (2010) Small molecule-capped gold nanoparticles as potent antibacterial agents that target gram-negative bacteria. J Am Chem Soc 132:12349–12356. doi:10.1021/Ja1028843